Scripta Materialia 181 (2020) 35–42

Contents lists available at ScienceDirect

Scripta Materialia

journal homepage: www.elsevier.com/locate/scriptamat

Viewpoint article

Strategy for managing both high strength and large ductility in structural materials–sequential nucleation of different deformation modes based on a concept of *plaston*

Nobuhiro Tsuji[a,b,*], Shigenobu Ogata[a,c], Haruyuki Inui[a,b], Isao Tanaka[a,b], Kyosuke Kishida[a,b], Si Gao[b], Wenqi Mao[b], Yu Bai[b], Ruixiao Zheng[b,d], Jun-Ping Du[a,c]

[a] *Elements Strategy Initiative for Structural Materials (ESISM), Kyoto University, Yoshida-honmachi, Sakyo-ku, Kyoto, 606-8501, Japan*
[b] *Department of Materials Science and Engineering, Kyoto University, Yoshida-honmachi, Sakyo-ku, Kyoto 606-8501, Japan*
[c] *Department of Mechanical Engineering and Bioengineering, Graduate School of Engineering Science, Osaka University, Toyonaka, 560-8531, Japan*
[d] *Key Laboratory of Aerospace Advanced Materials and Performance of Ministry of Education, School of Materials Science and Engineering, Beihang University, Beijing 100191, China*

ARTICLE INFO

Article history:
Received 14 August 2019
Revised 6 December 2019
Accepted 1 February 2020

Keywords:
Plastic instability
Strain hardening
Metallic materials
Deformation mode
Mechanical activation

ABSTRACT

Based on recent findings in ultrafine grained metals, we proposed a strategy for overcoming the strength-ductility trade-off in structural metallic materials. Sequential nucleation of different deformation modes, such as unusual slip systems, deformation twinning, martensitic transformation, etc., would regenerate strain-hardening ability of the material, leading to high strength and large tensile ductility. For discussing the activation of different deformation modes in atomistic scales, the concept of *plaston* which considered local excitation of atoms under singular dynamic fields was proposed.

Strength-ductility trade-off

Higher and higher strengths are required for structural materials in recent years, for reducing the weight of transportation machines like automobiles, realizing huge constructions, and securing human beings and society from accidents and disasters like collision, earthquake, and so on. However, the ductility and/or toughness of materials generally deteriorates with increasing the strength, as is schematically illustrated in Fig. 1(a) which is often called a “banana curve” due to its shape [1]. We need to overcome this trade-off relationship between strength and ductility/toughness, since high strength materials should be also manufactured into particular shapes and should avoid brittle or early fracture for maintaining safety in practical service. A number of publications have claimed findings of new materials managing both high strength and good ductility in the last decade [2–18]. However, most of them have mainly insisted superior mechanical properties found in different materials with different (and mostly complicated) microstructures, so that we still scarcely have general idea or principle to actively design advanced structural materials that can manage both high strength and ductility.

For overcoming the strength-ductility trade-off, we need to understand the fundamental reason for that. Let us now look at a typical example of the strength-ductility trade-off appearing in bulk nanostructured metals having ultrafine grained (UFG) microstructures. Fig. 1(b) shows engineering stress-strain curves at room temperature (RT) of an ultra-low carbon interstitial free (IF) steel [19] with various mean grain sizes ranging from 0.4 μm to 33 μm [20]. The single-phase microstructures of body-centered cubic (BCC) α ferrite with different grain sizes were fabricated by severe plastic deformation (SPD) using accumulative roll bonding (ARB) [21–23] and subsequent annealing [20]. The strength (especially the yield strength) of the material monotonously increased with decreasing the grain size, which could be understood in terms of the well-known Hall–Petch relationship [24,25]. On the other hand, the tensile ductility (especially the uniform elongation) of the material suddenly dropped when the average grain size became smaller than 1 μm. This is a strength-ductility trade-off appearing in most of UFG metals [26]. The outline of the stress-strain curves shown in Fig. 1(b) exhibits a “banana” shape. It should be also noted, by the way, that the specimens of which grain sizes were smaller than 2 μm showed discontinuous yielding characterized by

* Corresponding author at: Department of Materials Science and Engineering, Kyoto University, Yoshida-honmachi, Sakyo-ku, Kyoto 606-8501, Japan.
E-mail address: nobuhiro-tsuji@mtl.kyoto-u.ac.jp (N. Tsuji).

https://doi.org/10.1016/j.scriptamat.2020.02.001
1359-6462/

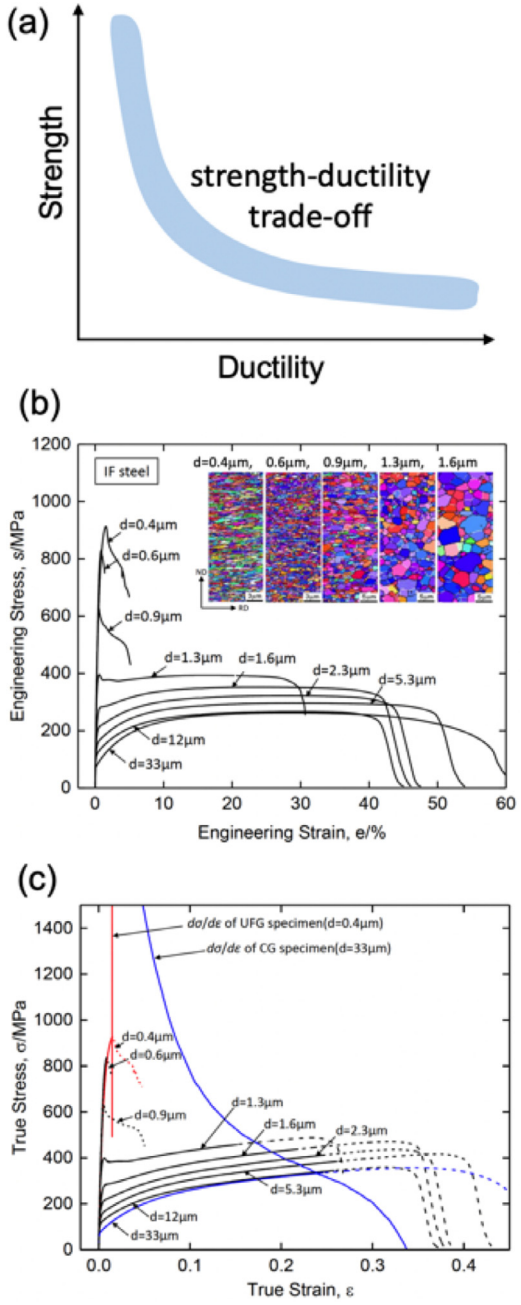

Fig. 1. (a) Schematic illustration showing the trade-off relationship between strength and ductility in materials (banana curve). (b) Engineering stress-strain curves at RT of the IF steel having various mean grain sizes (d) ranging from 0.4 μm to 33 μm, fabricated by SPD using ARB and subsequent annealing. EBSD-IPF maps showing typical grain structures are superimposed in the figure [19] (c) True stress-strain curves and corresponding strain-hardening curves of the IF steel specimens having various grain sizes. Stress-strain curves are drawn in solid lines up to the uniform elongation points determined from the engineering stress-strain curves, and then drawn in broken lines in post uniform elongation regions. Curves for the representatively coarse-grained ($d = 33$ μm) and UFG ($d = 0.4$ μm) specimen are expressed in blue and red, respectively. (For interpretation of the references to color in this figure legend, the reader is referred to the web version of this article.)

clear yield-drop, although the IF steel having no interstitial carbon and nitrogen normally shows continuous yielding [19]. It has been reported that UFG metals and alloys frequently show such a yield-drop phenomenon, regardless of kind and crystal structure of the materials [26–36].

The sudden decrease of ductility (especially uniform elongation) in UFG materials could be understood by plastic instability [26,37,38]. When necking happens in a tensile specimen, the tensile stress in the necked part becomes higher than that in the un-necked regions due to the decrease in the cross-sectional area. At the same time, however, the necked part is more strain-hardened than the un-necked regions. Therefore, whether the necking proceeds or not depends on the balance between the increased tensile stress and the increased hardness (strength) in the necked part. For strain-rate insensitive materials, a simple Considère criterion for plastic instability shown below is well known [39].

$$\left(\frac{d\sigma}{d\epsilon}\right) \leq \sigma \tag{1}$$

Here σ is the true flow stress and ε is the true strain, so that $(d\sigma/d\varepsilon)$ corresponds to the strain-hardening rate. The plastic instability condition determines the necking propagation, i.e., the uniform elongation in tensile tests. The Eq. (1) indicates that the strain-hardening rate $(d\sigma/d\varepsilon)$ plays a critical role for the plastic instability. Fig. 1(c) shows true stress-strain curves of the IF steel with various mean grain sizes, together with the strain-hardening rate curves for the specimens with $d = 33$ μm (blue) and $d = 0.4$ μm (red). The stress-strain curves are drawn in solid lines until the points of uniform elongation determined from the engineering stress-strain curves, and then drawn in broken lines for post-uniform elongation. In general, the strain-hardening rate monotonously decreases with the progress of plastic deformation, and eventually becomes lower than the flow stress, as is typically shown by the blue strain-hardening curve for the coarse-grained specimen in Fig. 1(c). The intersection corresponds to the plastic instability point. The strain at the intersection points corresponded well with the uniform elongation points of the specimens having average grain sizes over 1 μm. When the average grain size decreased down to 0.4 μm, the red strain-hardening curve quickly decreased and intersected with the stress-strain curve of the specimen at a very early stage of the tensile deformation. Although one of the reasons for the quick decrease in the strain-hardening rate in the UFG specimens was localized deformation accompanied with their yield-drop phenomenon [26,40], the strain-hardening rate did not recover afterward and the uniform elongation was limited below a few%. In grain refinement strengthening, there is usually no reason that the strain-hardening in finer grains are more enhanced than that in coarser grains, because structures at grain interior are the same. Since grain refinement primarily increases the yield strength of materials according to the Hall–Petch relationship [24], the early plastic instability described above seems indispensable in UFG metals.

Ultrafine grained materials managing both high strength and large ductility

Although many UFG metals exhibit the early plastic instability shown in Fig. 1, it has been found recently that several UFG materials show both high strength and large ductility [29,31–36]. Fig. 2 shows one example in an UFG Mg-Zn-Zr-Ca alloy [32,36]. Fully recrystallized microstructures having different mean grain sizes (d) ranging from 0.77 μm to 23.3 μm could be obtained in the Mg alloy after SPD using high pressure torsion (HPT) [41] and subsequent annealing. Typical UFG ($d = 0.77$ μm) and coarse-grained ($d = 23.3$ μm) structures are exhibited in Fig. 2 (a-1) and (a-2), respectively. True stress-strain curves of the specimens having the grain sizes of 0.77 μm (red) and 23.3 μm (blue) are shown in Fig. 2(b), together with corresponding strain-hardening rate curves. The yield strength of the Mg alloy significantly increased from 90 MPa to 235 MPa by the grain refinement from 23.3 μm to 0.77 μm [32]. The shape of the stress-strain curve around

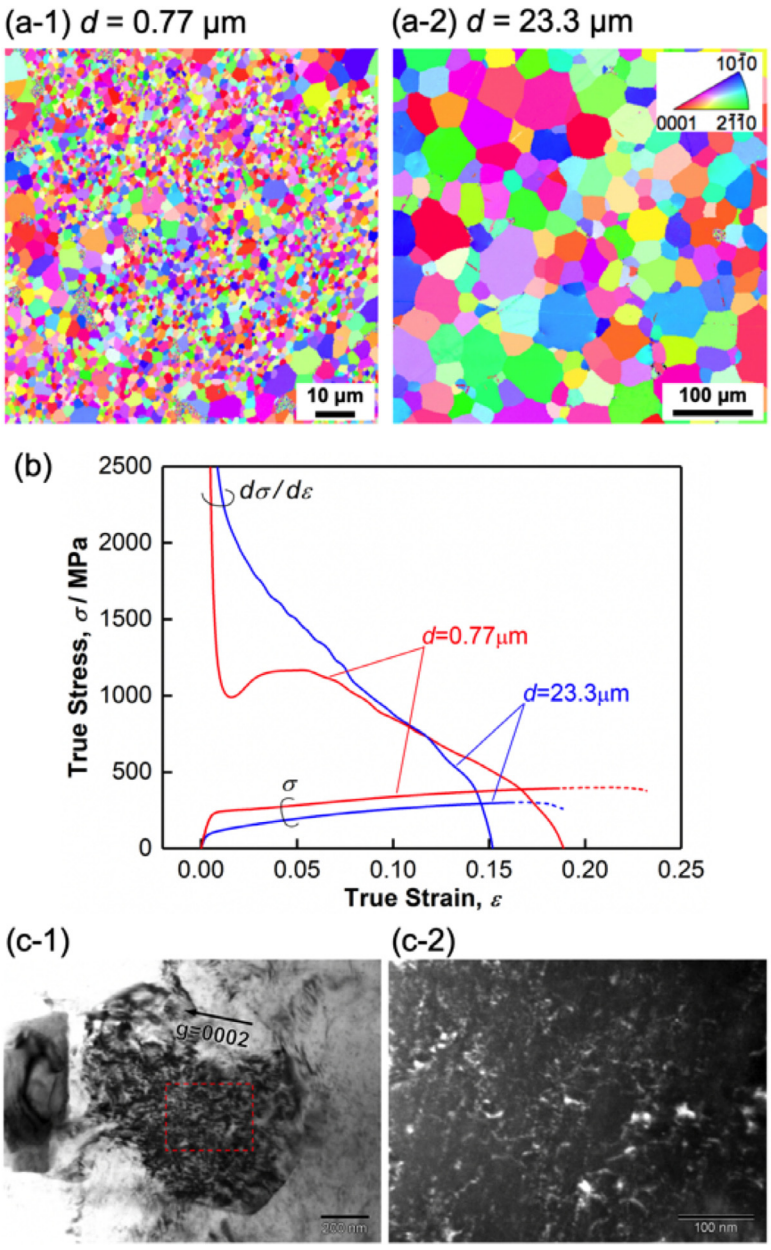

Fig. 2. (a) EBSD-IPF maps of the fully recrystallized structures having the mean grain sizes (d) of 0.77 μm (a-1) and 23.3 μm (a-2) in Mg-Zn-Ca-Zr alloy (ZKX600) processed by SPD using HPT and subsequent annealing. [32] (b) True stress-strain curves at RT and corresponding strain-hardening curves of the Mg alloy specimens having the average grain size of 0.77 μm (red) and 23.3 μm (blue). (c) TEM images of the UFG Mg alloy specimen ($d = 0.77$ μm) after a tensile deformation to 9.5%. A TEM bright-field image observed from near [01–10] zone axis under a two-beam condition (c-1) and a corresponding dark-field image using $g = 0002$ (c-2). [36] (For interpretation of the references to color in this figure legend, the reader is referred to the web version of this article.)

yielding changed from continuous one to discontinuous-like one by the grain refinement. It should be noted that the UFG specimen showed good strain-hardening ability even after the high yield strength, and exhibited higher tensile strength (328 MPa) as well as larger uniform and total elongations (20.5% and 26.1%, respectively) than the coarse-grained specimen (256 MPa, 17.6%, and 20.3%). The red strain-hardening curve for the 0.77 μm specimen quickly dropped at the beginning of deformation corresponding to the discontinuous yielding, but the strain-hardening rate then regenerated again to show high values comparable to (or even higher at later stage than) that for the coarse-grained (23.3 μm) specimen. As a result, the plastic instability was postponed and both high strength and large ductility were realized in the UFG specimen. Fig. 2 (c-1) and (c-2) show a TEM bright-field image observed from near [01–10] zone axis under a two-beam condition and a corresponding dark-field image using $\boldsymbol{g} = 0002$, respectively, for the UFG specimen after a tensile strain of 9.5% [36]. In Mg and Mg alloys having hexagonal close-pack (HCP) structure, it is well known that basal slips having Burgers vector ($\boldsymbol{b}$) parallel to $<\boldsymbol{a}>$ axis in HCP crystal preferentially occur at ambient temperature [42]. However, many dislocations in Fig. 2 (c-2) show clear bright contrast, indicating that those dislocations have Burgers vector with $<\boldsymbol{c}>$ component. They are considered to be $<\boldsymbol{c}+\boldsymbol{a}>$ dislocations probably belonging to a pyramidal slip system. Operation of such a different slip system in addition to usual basal slip would increase the chance of interactions between operated dislocations and inhibit annihilation of dislocations, resulting in enhanced strain-hardening shown in Fig. 2(b). That is, unusual $<\boldsymbol{c}+\boldsymbol{a}>$ dis-

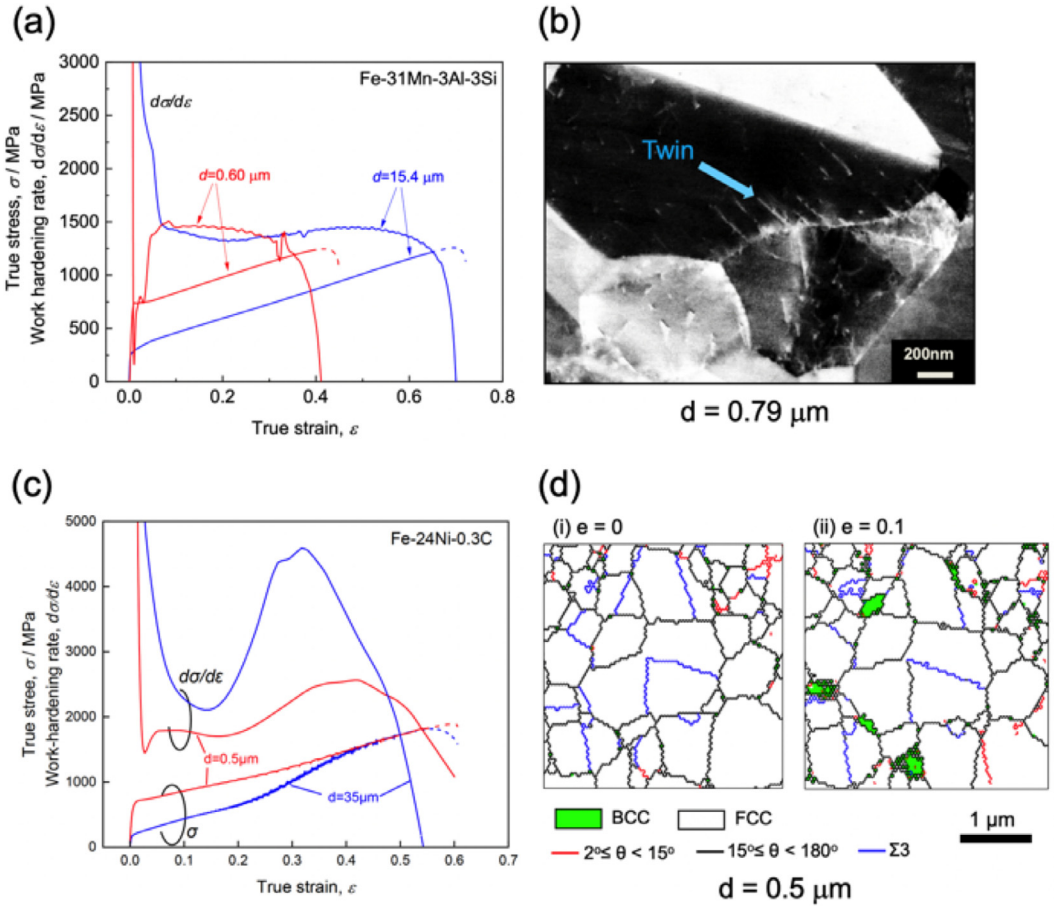

Fig. 3. (a) True stress-strain curves at RT and corresponding strain-hardening curves of the 31Mn-3Al-3Si austenitic steel having the average grain size (d) of 0.60 μm (red) and 15.4 μm (blue). (b) SEM-ECCI image of the 31Mn-3Al-3Si steel with an UFG grain size ($d = 0.79$ μm) after 1.6% tensile deformation. Nucleation of deformation twins from grain boundaries is observed. [44] (c) True stress-strain curves at RT and corresponding strain-hardening curves of the 24Ni-0.3C metastable austenitic steel having the average grain size of 0.5 μm (red) and 35 μm (blue). (d) EBSD grain boundary and phase maps of the 24Ni-0.3C steel having the UFG grain size ($d = 0.5$ μm) after a tensile deformation to a strain (e) of 0.1 (10%). High-angle grain boundaries having misorientations (θ) larger than 15° and low-angle grain boundaries with $2° \leqq \theta < 15°$ are drawn in black lines and red lines, respectively. Annealing twin boundaries (Σ3) are drawn in blue. Austenite mother phase with FCC structure and martensite phase with BCC structure are painted in white and green, respectively. Nucleation of deformation induced martensite (green regions) from grain boundaries are observed. (For interpretation of the references to color in this figure legend, the reader is referred to the web version of this article.)

locations were unexpectedly activated in the UFG Mg alloy, which was the reason for the regeneration of strain-hardening leading to both high strength and large ductility.

Fig. 3 shows another type of examples in different kinds of UFG materials overcoming the strength-ductility trade-off. Fig. 3 shows true stress-strain curves at RT and corresponding strain-hardening curves of the fully recrystallized specimens of an 31Mn-3Al-3Si (mass%) steel having average grain sizes of 15.4 μm (blue) and 0.60 μm (red), fabricated by conventional heavy cold-rolling and appropriate annealing [29,43]. The steel maintained a fully austenitic (face centered cubic: FCC) structure at room temperature. Similar to the Mg alloy shown in Fig. 2, the yield strength of this alloy greatly increased by the grain refinement, but the strain-hardening rate of the 0.60 μm specimen regenerated after the quick drop at discontinuous yielding and maintained high values comparable to that of the coarse-grained specimen. As a result, high tensile strength (836 MPa) and large uniform elongation (43.3%) were achieved in the UFG 31Mn-3Al-3Si steel. An electron channeling contrast image (ECCI) taken by scanning electron microscopy (SEM) of the UFG specimen after a tensile strain of 1.6% is shown in Fig. 3(b) [44]. At this early stage of deformation, it was observed that deformation twins nucleated from grain boundaries in the UFG specimen. By the way, it is well known that deformation twinning in FCC metals and alloys becomes difficult to occur with decreasing grain size [45], which could be understood by less chances of the dislocation reactions for producing deformation twins [46] in the finer grains. It is noteworthy, therefore, that deformation twinning was rather enhanced in the UFG specimen with sub-micrometer grain sizes and they were nucleated from grain boundaries (not by the dislocation interactions in grains). Consequently, such deformation twins were considered to be responsible to the enhanced strain-hardening ability leading to the high strength and large ductility.

True stress-strain curves at RT and strain-hardening rate curves of a metastable austenitic (FCC) steel, Fe-24Ni-0.3C (mass%), having different grain sizes ($d = 35$ μm (blue) and 0.5 μm (red)) are shown in Fig. 3(c). The specimens with fully recrystallized microstructures with different mean grain sizes were fabricated by conventional heavy cold-rolling and appropriate annealing. In this material, strain-hardening was significantly regenerated even in the conventionally coarse-grained ($d = 35$ μm) specimen, as shown by the blue curve of strain-hardening rate in Fig. 3(c), which was attributed to the deformation induced martensitic transformation. The resultant high strength and large ductility in such metastable austenitic alloys are called transformation induced plasticity (TRIP) [47]. It should be noted here that grain refinement stabilizes the mother phase (austenite) against martensitic transformation [48]. In fact, the martensitic transformation starting temperature (Ms)

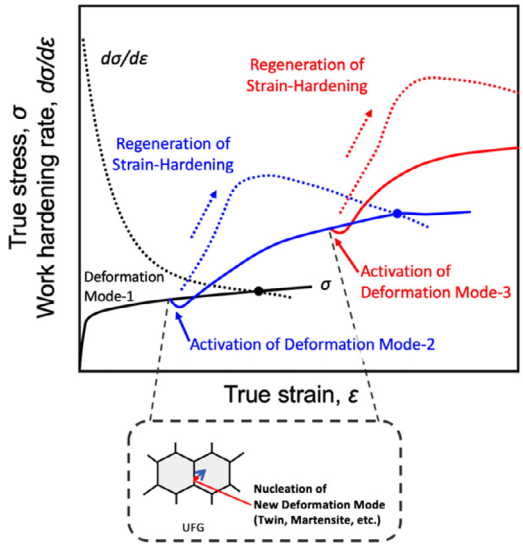

Fig. 4. Schematic illustration showing a strategy for managing both high strength and large ductility of the materials through sequential nucleation (activation) of different deformation modes and regeneration of strain-hardening ability. An illustration showing the nucleation of a new deformation mode from a grain boundary in UFG materials is shown at lower position, as an example of such a nucleation.

in cooling of this alloy decreased from −26 °C to −66 °C by the grain refinement from 35 μm to 0.5 μm [49,50]. Even though the austenite was stabilized by the grain refinement, the UFG specimen ($d = 0.5$ μm) showed deformation induced martensite with body centered cubic (BCC) structure (painted in green in Fig. 3(d)) nucleated from grain boundaries of austenite, after a tensile strain (e) of 0.1 (10%). Consequently the strain-hardening rate increased again after the early drop, postponing plastic instability and resulting in high strength and large ductility even in the UFG specimen, as was shown in Fig. 3(c).

Strategy to overcome strength-ductility trade-off and a concept of *plaston*

The results in the UFG metals described above clearly indicate a possibility to overcome the strength-ductility trade-off. In each example, different deformation modes, i.e., <***c***+***a***> dislocations in the Mg alloy, deformation twin in the high-Mn austenitic steel, or martensite in the metastable austenitic steel, were unexpectedly activated to enhance and regenerate strain-hardening. After such evidences, we would like to claim a strategy for managing high strength and large ductility in advanced high strength structural metals, as is illustrated in Fig. 4. Even a normal operation of single deformation mode (like normal dislocation slip) causes strain-hardening, but the strain-hardening rate decreases monotonously with increasing the plastic strain. If a different deformation mode is activated (deformation mode-2 in Fig. 4), the strain-hardening ability can be regenerated probably due to interactions between different deformation modes (or resultant lattice defects of different types), leading to postponing plastic instability. If different deformation modes are sequentially activated, the strain-hardening ability is regenerated at all such times, leading to high strength and large ductility, as is illustrated in Fig. 4.[1] A schematic illustration showing a nucleation of new deformation mode from a grain boundary in UFG metals observed above (Fig. 3) is also shown as an example of such an activation.

Why were the unusual deformation modes activated in some UFG materials? We think that the normal deformation mode (i.e., normal dislocation slips) became difficult to operate within fully recrystallized ultrafine grains having limited volumes. Similar phenomena have been reported after micro-pillar experiments in the last decade [51–54]. When the size of the micro-pillar single crystals of various kinds of materials fabricated by focused ion beam (FIB) processing decreased below a few micro-meters, their strengths greatly increased [51–60]. This has been explained by the so-called dislocation source hardening [53,54,61,62]. Metallic materials maintain a relatively large number of dislocations even after annealing, so that coarse crystals generally involve easy dislocation sources (like Frank–Read source [63]) as well as pre-existing mobile dislocations. Therefore, coarse crystals do not need to newly nucleate dislocations to initiate plastic deformation. When the crystal size decreases very much, the fine crystals might not include any dislocation sources stochastically, leading to high yield strength sometimes approaching to the ideal strength of the crystal [54,64–71]. It would be reasonable to consider that similar thing can happen in polycrystalline grains having sub-micrometer grain sizes. We think that the yield-drop phenomenon and discontinuous yielding that have been observed in fully recrystallized UFG metals regardless of the kind of materials [26–36] reflects such a situation, since it is well known that the yield-drop phenomenon generally happens when free (mobile) dislocations are deficient in crystals [72]. For initiating or developing plastic deformation in such UFG metals, any carriers of plastic deformation have to be nucleated. The nucleation must occur from grain boundaries, as was indeed shown in UFG Mg, UFG austenitic steel and UFG metastable austenitic steel that nucleated <***c***+***a***> dislocations, deformation twins, and martensite, respectively (Figs. 2 and 3). In case of micro pillars, nucleation of deformation modes initiate most likely from the surfaces [73–76]. High stress conditions realized upon such circumstances lacking free dislocations or dislocation sources must be one of the reasons for the nucleation of unusual deformation modes. We consider that dislocations were newly nucleated even in the UFG IF steel as well (Fig. 1), but only the operation of the same (single) deformation mode could not enhance strain-hardening due to the lack of interaction between different deformation modes or lattice defects, leading to the limited tensile ductility.

The details of the reason why the strain-hardening was regenerated by the operation of different deformation modes are still unclear. High-Mn steels and metastable austenitic (Ni-C) steels are originally known to show good balances of strength and ductility even in conventionally coarse grain sizes [1]. Their good mechanical properties have been considered due to deformation twinning or deformation induced martensitic transformation, which have been named twinning induced plasticity (TWIP) [77,78] or TRIP [47], respectively. However, the mechanisms of enhanced strain-hardening have not yet been exactly clarified even for the conventional TWIP and TRIP phenomena [79]. Another critical point unknown and to be clarified is the activation (nucleation) mechanism of different deformation modes [80]. Without understanding the activation mechanism, we cannot design metallic materials having appropriate chemical compositions and microstructures for sequentially activating different deformation modes and enhancing strain-hardening as expressed in Fig. 4. For considering the activation of deformation modes generally, we should consider the

[1] Strictly speaking, the initiation of new deformation modes releases elastic energy stored in the material, so that the flow stress might decrease at that moment, which is somehow reflected in Fig.4. This corresponds to the yield-drop phenomenon in fully recrystallized UFG materials, as is discussed in the next section. Such a drop of the stress might be veiled in bulky materials having heterogeneities in microstructures, but may appear more obviously in nano-scale materials. Whether such a stress-drop appears on the global stress-strain curve or not would also depend on the nucleation kinetics of the new deformation mode as well as the degree of heterogeneity of its appearance in the material.

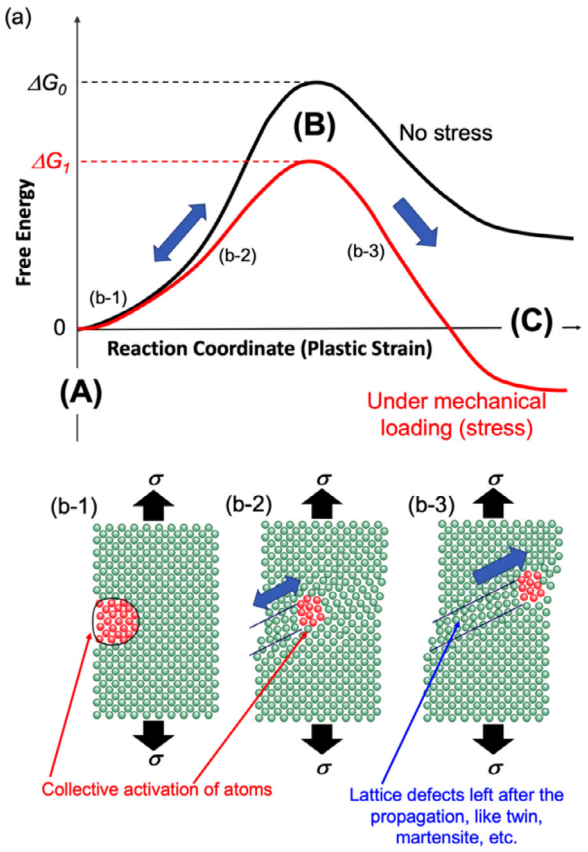

Fig. 5. (a) Changes in the free energy of the system (material) during the nucleation of a deformation mode according to the reaction coordinate (collective valuable), the plastic strain in this case. Two different free energy curves are drawn, corresponding to a case without stress (black) and a case under a stress (red), respectively. (b) Schematic illustrations showing changes of atomistic structures in a crystal, corresponding to different stages of nucleation shown in (a). Red atoms correspond to the "*plaston*", i.e., the local defective region collectively activated mechanically and thermally at a singular region in the material. The propagation of the *plaston* brings about plastic deformation and may leave a particular lattice defects, such as stacking faults, deformation twins, martensite, etc. (For interpretation of the references to color in this figure legend, the reader is referred to the web version of this article.)

energetics and kinetics of the deformation mode under a mechanical loading (stress), as illustrated in Fig. 5. Fig. 5(a) shows changes in the free energy of the system (material) during the activation of a deformation mode according to the reaction coordinate (collective valuable), i.e., the plastic strain in this case. Fig. 5(b) illustrates changes of local atomistic structures in a crystal, corresponding to different stages in Fig. 5(a). Fig. 5 (b-1) and (b-2) exhibit the status between the initial point (A) and the peak-energy point (B) in Fig. 5(a), and Fig. 5 (b-3) indicates that between the point (B) and the point (C) in Fig. 5(a). In Fig. 5(a), two different free energy curves are drawn, corresponding to a case without stress (black) and a case under a stress (red), respectively. In both cases, the material needs to overcome an energy barrier (ΔG) for the activation. When no stress is applied, only thermal activation can overcome the barrier (ΔG_0). However, the resultant state (C) should have higher free energy than the initial state (A) because of lattice defects introduced by the plastic deformation (such as, dislocations, surface steps, deformation twins, martensite crystals, and so on), so that the reaction from (A) to (C) via (B) cannot spontaneously happens without mechanical loading (stress). When a stress is applied to the material, the activation barrier is reduced from ΔG_0 to ΔG_1, by the mechanical activation. Correspondingly, it should be noted that the final state (C) becomes lower than the initial state (A) in this case, because of a release of an energy by the plastic deformation realized. This means that a driving force from (A) to (C) arises under a stress. Let us here consider the change of local atomistic structures during the process in Fig. 5(b). Here, a perfect crystal without any lattice defects that can be carriers of plastic deformation (like dislocations) is considered. In such a case, we need to nucleate the new deformation mode that leads to a plastic deformation for relaxing the stress. At a singular region with high local stress and/or high energy in the material, such as grain/phase boundary, surface, crack tip, etc., a certain group of atoms would be activated mechanically and thermally, and form a defective zones (drawn by red atoms in Fig. 5(b)). Migration of the local defective zone results in a plastic strain. Between the states (A) and (B) before the energy barrier in Fig. 5(a), the defective zone may migrate back and forth. After overcoming the barrier (ΔG_1), however, the defective zone migrates in one direction to produce further plastic deformation. The formation and migration of such a local defective zone is the elemental process for the nucleation of a new deformation mode. The propagation of the defective zone may leave a particular defect, such as a stacking fault, deformation twin, martensite, rejuvenated glass and so on, depending on the type of the deformation mode. We would like to call such a localized defective zone of excited atomic structure (expressed by red atoms in Fig. 5(b)) "*plaston*", since it is the essential structure that leads to a plastic strain by its migration. Atomistic structure in dislocation core is one of such localized defective zones.

As was mentioned above, enhancement of both strength and ductility by deformation twinning and deformation-induced martensitic transformation has been already known as TWIP [77,78] and TRIP [47], respectively. However, we cannot yet actively control TRIP and TWIP, since we still do not know the critical atomistic process of nucleation for deformation twinning and deformation-induced martensitic transformation. Additionally, we think that it has not yet been clearly proved why global strain-hardening of materials is enhanced by deformation twinning (TWIP) and martensitic transformation (TRIP). Dislocation theory is powerful to explain plastic deformation and strength of metallic materials, but has a limitation. The dislocation theory is based on elastic fields around dislocations, but the elastic fields of dislocations are obtained assuming Volterra's hollow cylinder [63]. Therefore, the dislocation theory does not treat discrete atomistic information. As a result, we cannot yet discuss the nucleation of dislocations. Nucleation and growth of deformation twins (especially in FCC crystals) and martensite have been often described by movement of partial or interfacial dislocations and reactions of dislocations, which are, however, just based on geometry. It is also well known that twins and martensite preferentially nucleate from grain boundaries. In the present paper, indeed, we have shown that deformation twins, martensite and ***c+a*** dislocations in HCP Mg alloys nucleated from grain boundaries in ultrafine grained metals (Figs. 2 and 3), which cannot be described by the dislocation theory. We need to understand elementary processes for those phenomena in atomistic scales with their thermodynamics and kinetics, in order to control the sequential nucleation illustrated in Fig. 4.

The *plaston* expressed in Fig. 5 does describe such atomistic processes. We believe that the concept of *plaston* expressed in Fig. 5 is useful for various kinds of plastic phenomena, i.e., the nucleation and migration of dislocations [81], deformation twins [82,83], martensite, disclination, dislocation loops [65,84–87], disconnections/ledges/steps on grain boundary/interface [88,89], vacancy/interstitial clusters, shear transformation in glass [90–93], and other unknown things in atomistic scales. Experimental analyses and computer simulations in atomistic scale considering *plaston* would deepen the understanding of activation and migration properties of the localized defective zone (*plaston*) that produces plasticity. Different kinds of *plaston* would have different activation

energies and different dependencies on stress and temperature. Once we figure out those properties, we would be able to design optimized material with appropriate chemical compositions and microstructures and to realize optimized processes at appropriate temperature and strain rate for controlling the activation of different deformation modes. The concept of *plaston* would be also useful for considering fatigue and fracture behavior of materials, since regions near crack-tips are typical singular points of stress. Then it would become possible not only to overcome the strength-ductility trade-off but also to make less deformable materials plastic.

Summary

In summary, some actual examples of UFG materials that could overcome the strength-ductility trade-off were introduced in the early part of this paper. Each UFG metal showed an unexpected activation of different deformation modes, which regenerated the strain-hardening ability of the materials, leading to high strength and large ductility. Based on the results, a strategy, i.e., sequential nucleation of different deformation modes for regenerating and sustaining high strain-hardening rate, was proposed. In order to consider the fundamental principle of the nucleation (or activation) of different deformation modes, we also proposed a concept of *plaston*, as a local defective region composed of collectively activated (or excited) atoms to create plasticity of the materials. Understanding of the *plaston* concept would make it possible to design advanced structural materials controlling the activation of various deformation modes in appropriate timing, and would give a fundamental principle for managing both high strength and large ductility.

Declaration of Competing Interests

The authors declare that they have no known competing financial interests or personal relationships that could have appeared to influence the work reported in this paper.

Acknowledgments

The authors gratefully appreciate the financial support for the Elements Strategy Initiative for Structural Materials (ESISM) at Kyoto University by the Ministry of Education, Culture, Sports, Science and Technology (MEXT) (project number JPMXP0112101000), Japan. NT was also supported by JST CREST (JPMJCR1994). We also would like to thank Prof. T. Shimokawa of Kanazawa University and Prof. K. Tsuzaki of Kyushu University for their valuable comments and suggestions.

References

[1] M.Y Demeri, Advanced High-Strength Steels: Science, Technology, and Applications, ASM International, Materials Park, Ohio, 2013.
[2] Y.H. Zhao, X.Z. Liao, S. Cheng, E. Ma, Y.T. Zhu, Adv. Mater. 18 (2006) 2280–2283.
[3] L. Lu, X. Chen, X. Huang, K. Lu, Science 323 (2009) 607–610.
[4] N. Copper, T.H. Fang, W.L. Li, N.R. Tao, K. Lu, Science 331 (2011) 1587–1590.
[5] G. Liu, G.J. Zhang, F. Jiang, X.D. Ding, Y.J. Sun, J. Sun, E. Ma, Nat. Mater. 12 (2013) 344–350.
[6] X. Wu, P. Jiang, L. Chen, F. Yuan, Y.T. Zhu, Proc. Natl. Acad. Sci. 111 (2014) 7197–7201.
[7] Y. Wei, Y. Li, L. Zhu, Y. Liu, X. Lei, G. Wang, Y. Wu, Z. Mi, J. Liu, H. Wang, H. Gao, Nat. Comm. 5 (2014) 3580.
[8] S.-.H. Kim, H. Kim, N.J. Kim, Nature 518 (2015) 77–79.
[9] X. Wu, M. Yang, F. Yuan, G. Wu, Y. Wei, X. Huang, Y. Zhu, Proc. Natl. Acad. Sci. 112 (2015) 14501–14505.
[10] Z. Li, K.G. Pradeep, Y. Deng, D. Raabe, C.C. Tasan, Nature 534 (2016) 227–230.
[11] B.B. He, B. Hu, H.W. Yen, G.J. Cheng, Z.K. Wang, H.W. Luo, M.X. Huang, Science 357 (2017) 1029–1032.
[12] E. Ma, T. Zhu, Mater. Today 20 (2017) 323–331.
[13] L. Liu, Q. Ding, Y. Zhong, J. Zou, J. Wu, Y.L. Chiu, J. Li, Z. Zhang, Q. Yu, Z. Shen, Mater. Today 21 (2018) 354–361.
[14] Z. Lei, X. Liu, Y. Wu, H. Wang, S. Jiang, S. Wang, X. Hui, Y. Wu, B. Gault, P. Kontis, D. Raabe, L. Gu, Q. Zhang, H. Chen, H. Wang, J. Liu, K. An, Q. Zeng, T.G. Nieh, Z. Lu, Nature 563 (2018) 546–550.
[15] Y. Tong, Y.L. Zhao, A. Hu, K. Lu, J.X. Cai, J.J. Kai, Y. Liu, T. Yang, J. Wei, C.T. Liu, X.D. Han, Z.B. Jiao, D. Chen, Science 362 (2018) 933–937.
[16] M. Yang, D. Yan, F. Yuan, P. Jiang, E. Ma, X. Wu, Proc. Natl. Acad. Sci. 115 (2018) 7224–7229.
[17] W. Sun, Y. Zhu, R. Marceau, L. Wang, Q. Zhang, X. Gao, C. Hutchinson, Science 363 (2019) 972–975.
[18] J. Zhang, I.J. Beyerlein, W. Han, Phys. Rev. Lett. 122 (2019) 255501.
[19] H. Takechi, ISIJ Int. 34 (1994) 1–8.
[20] S. Gao, M. Chen, S. Chen, N. Kamikawa, A. Shibata, N. Tsuji, Mater. Trans. 55 (2014) 73–77.
[21] Y. Saito, N.T. suji, H. Utsunomiya, T. Sakai, R.G. Hong, Scripta Mater. 39 (1998) 1221–1227.
[22] Y. Saito, H. Utsunomiya, N. Tsuji, T. Sakai, Acta Mater. 47 (1999) 579–583.
[23] N. Tsuji, Y. Saito, S.H. Lee, Y. Minamino, Adv. Eng. Mater. 5 (2003) 338–344.
[24] E.O. Hall, Proc. Phys. Soc. Lond. B 64 (1951) 742–747.
[25] N.J. Petch, J. Iron Steel Inst. 174 (1953) 25–28.
[26] N. Tsuji, Y. Ito, Y. Saito, Y. Minamino, Scripta Mater. 47 (2002) 893–899.
[27] D. Terada, M. Inoue, H. Kitahara, N. Tsuji, Mater. Trans. 49 (2008) 41–46.
[28] N. Kamikawa, X. Huang, N. Tsuji, N. Hansen, Acta Mater. 57 (2009) 4198–4208.
[29] R. Saha, R. Ueji, N. Tsuji, Scripta Mater. 68 (2013) 813–816.
[30] S. Gao, A. Shibata, M. Chen, N. Park, N. Tsuji, Mater. Trans. 55 (2014) 69–72.
[31] Y.Z. Tian, A. Shibata, Z.F. Zhang, N. Tsuji, Mater. Res. Lett 4 (2016) 112–117.
[32] R. Zheng, T. Bhattacharjee, A. Shibata, T. Sasaki, K. Hono, M. Joshi, N. Tsuji, Scripta Mater. 131 (2017) 1–5.
[33] S. Yoshida, T. Bhattacharjee, Y. Bai, N. Tsuji, Scripta Mater. 134 (2017) 33–36.
[34] Y.Z. Tian, S. Gao, L.J. Zhao, S. Lu, R. Pippan, Z.F. Zhang, N. Tsuji, Scripta Mater. 142 (2018) 88–91.
[35] S. Yoshida, T. Ikeuchi, T. Bhattacharjee, Y. Bai, A. Shibata, N. Tsuji, Acta Mater. 171 (2019) 201–215.
[36] R. Zheng, T. Bhattacharjee, S. Gao, W. Gong, A. Shibata, T. Sasaki, K. Hono, N. Tsuji, Sci. Rep. 9 (2019) 11702.
[37] Y. Wang, M. Chen, F. Zhou, E. Ma, Nature 419 (2002) 912.
[38] J.W. Morris Jr, ISIJ Int. 48 (2008) 1063–1070.
[39] R.H. Wagoner, J.L. Chenot, Fundamentals of Metal Formong, John Wiley & Suns, New York, 1997.
[40] S. Gao, Y. Bai, R. Zheng, Y.Z. Tian, W. Mao, A. Shibata, N. Tsuji, Scripta Mater. 159 (2019) 28–32.
[41] A. Azushima, R. Kopp, A. Korhonen, D.Y. Yang, F. Micari, G.D. Lahoti, P. Groche, J. Yanagimoto, N. Tsuji, A. Rosochowski, A. Yanagida, SIRP Annals 57 (2008) 716–735.
[42] H. Yoshinaga, R. Horiuchi, Trans. JIM 5 (1964) 14–21.
[43] Y. Bai, Y. Momotani, M.C. Chen, A. Shibata, N. Tsuji, Mater. Sci. Eng. A 651 (2016) 935–944.
[44] H. Kitamura, Master thesis, Kyoto University, 2017.
[45] E.E.-D. Surya, R. Kalidindi, R.D. Doherty, Metall. Mater. Trans. A 30 (1999) 1223–1233.
[46] S. Miura, J. Takamura, N. Narita, Trans. JIM 9 (1968) 555–561.
[47] V.F. Zackay, E.R. Parker, D. Fahr, R. Bush, Trans. ASM 60 (1967) 252–259.
[48] M. Umemoto, W.S. Owen, Metall. Trans. 5 (1974) 2041–2046.
[49] S. Chen, A. Shibata, S. Gao, N. Tsuji, Mater. Trans. 55 (2014) 223–226.
[50] S. Chen, Ph.D. thesis, Kyoto University, 2015.
[51] M.D. Uchic, D.M. Dimiduk, J.N. Florando, W.D. Nix, Science 305 (2004) 986–989.
[52] J.R. Greer, W.C. Oliver, W.D. Nix, Acta Mater. 53 (2005) 1821–1830.
[53] M.D. Uchic, P.A. Shade, D.M. Dimiduk, Ann. Rev. Mater. Res. 39 (2009) 361–386.
[54] O. Kraft, P.A. Gruber, R. Mönig, D. Weygand, Ann. Rev. Mater. Res. 40 (2010) 293–317.
[55] K. Fujimura, K. Kishida, K. Tanaka, H. Inui, MRS Symp. Proc. 1295 (2011) 201–206.
[56] A. Inoue, K. Kishida, H. Inui, K. Hagihara, MRS Symp. Proc. 1516 (2013) 151–156.
[57] Z.M.T. Chen, N.L. Okamoto, M. Demura, H. Inui, Scripta Mater. 121 (2016) 28–31.
[58] N.L. Okamoto, S. Fujimoto, Y. Kambara, M. Kawamura, Z.M.T. Chen, H. Matsunoshita, K. Tanaka, H. Inui, E.P. George, Sci. Rep. 6 (2016) 35863.
[59] J. Zhang, K. Kishida, H. Inui, Int. J. Plast. 92 (2017) 45–56.
[60] M. Higashi, S. Momono, K. Kishida, N.L. Okamoto, H. Inui, Acta Mater. 161 (2018) 161–170.
[61] T.A. Parthasarathy, S.I. Rao, D.M. Dimiduk, M.D. Uchic, D.R. Trinkle, Scripta Mater. 56 (2007) 313–316.
[62] S.W. Lee, W.D. Nix, Philos. Mag. 92 (2012) 1238–1260.
[63] Peter M Anderson, John P. Hirth, Jens Lothe, Theory of Dislocations, 3rd ed., Cambridge University Press, New York, 2017.
[64] H. Bei, S. Shim, G.M. Pharr, E.P. George, Acta Mater 56 (2008) 4762–4770.
[65] T. Zhu, J. Li, A. Samanta, A. Leach, K. Gall, Phys. Rev. Lett. 100 (2008) 025502–1-4.
[66] A.T. Jennings, C.R. Weinberger, S.W. Lee, Z.H. Aitken, L. Meza, J.R. Greer, Acta Mater. 61 (2013) 2244–2259.
[67] P. Sudharshan Phani, K.E. Johanns, E.P. George, G.M. Pharr, Acta Mater. 61 (2013) 2489–2499.
[68] S. Ogata, Ju. Li, S. Yip, Science 298- (2002) 807–811.
[69] S. Ogata, J. Li, N. Hirosaki, Y. Shibutani, Phys. Rev. B 70 (2004) 104104.
[70] T. Zhu, J. Li, S. Ogata, S. Yip, MRS Bull. 34 (2009) 167–172.

[71] T. Zhu, J. Li, Prog. Mater. Sci. 55 (2010) 710–757.
[72] E.O. Hall, Yield Point Phenomena in Metals & Alloys, Plenum Press, New York, 1970.
[73] N.L. Okamoto, D. Kashioka, M. Inomoto, H. Inui, H. Takebayashi, S. Yamaguchi, Scripta Mater. 69 (2013) 307–310.
[74] N.L. Okamoto, M. Inomoto, H. Adachi, H. Takebayashi, H. Inui, Acta Mater. 65 (2014) 229–239.
[75] S. Nakatsuka, K. Kishida, H. Inui, in: Proceedings of the MRS Symposium, 1760, 2015 mrsf14-1760-yy05-09.
[76] K. Kishida, T. Maruyama, H. Matsunoshita, T. Fukuyama, H. Inui, Acta Mater. 159 (2018) 416–428.
[77] O. Grässel, L. Kruger, G. Frommeyer, L. Meyer, Int. J. Plast. 16 (2000) 1391–1409.
[78] B.C. De Cooman, Y. Estrin, S.K. Kim, Acta Mater. 142 (2018) 283–362.
[79] Z.C. Luo, M.X. Huang, Scripta Mater. 142 (2018) 28–31.
[80] J. Li, MRS Bull. 32 (2007) 151–159.
[81] S. Shinzato, M. Wakeda, S. Ogata, Int. J. Plast. 122 (2019) 319–337.
[82] S. Ogata, J. Li, S. Yip, Phys. Rev. B 71 (2005) 224102.
[83] A. Ishii, J. Li, S. Ogata, Int. J. Plast. 82 (2016) 32–43.
[84] T. Zhu, J. Li, A. Samanta, H. G.Kim, S. Suresh, Proc. Natl. Acad. Sci. 104 (2007) 3031–3036.
[85] J.-.P. Du, Y.-J. Wang, Y.-.C. Lo, L. Wan, S. Ogata, Phys. Rev. B 94 (2016) 104110.
[86] Q.-J. Li, B. Xu, S. Hara, J. Li, E. Ma, Acta Mater. 145 (2018) 19–29.
[87] Y. Sato, S. Shinzato, T. Ohmura, S. Ogata, Int. J. Plast. 121 (2019) 280–292.
[88] N. Combe, F. Mompiou, M. Legros, Phys. Rev. B 93 (2016) 024109.
[89] O. MacKain, M. Cottura, D. Rodney, E. Clouet, Phys. Rev. B 95 (2017) 134102.
[90] F. Shimizu, S. Ogata, J. Li, Acta Mater. 54 (2006) 4293–4298.
[91] F. Shimizu, S. Ogata, J. Li, Mater. Trans. 48 (2007) 2923–2927.
[92] P. Zhao, J. Li, Y. Wang, Int. J. Plast. 40 (2013) 1–22.
[93] F. Boioli, T. Albaret, D. Rodney, Phys. Rev. E 95 (2017) 033005.